Structural Organization of the N-Terminal Domain of Apolipoprotein A-I: Studies of Tryptophan Mutants†

W. Sean Davidson,‡,§ Kirsten Arnvig-McGuire,‡ Adam Kennedy,‡ Jeff Kosman,‡ Theodore L. Hazlett,|| and Ana Jonas*,‡

Department of Biochemistry, College of Medicine at Urbana−Champaign, University of Illinois, 506 South Mathews Avenue, Urbana, Illinois 61801, and Laboratory for Fluorescence Dynamics, Department of Physics, University of Illinois at Urbana−Champaign, 1110 West Green Street, Urbana, Illinois 61801

Received June 22, 1999; Revised Manuscript Received August 12, 1999

ABSTRACT: Site-directed mutagenesis and detailed fluorescence studies were used to study the structure and dynamics of recombinant human proapolipoprotein (proapo) A-I in the lipid free state and in reconstituted high-density lipoprotein (rHDL) particles. Five different mutants of proapoA-I, each containing a single tryptophan residue, were produced in bacteria corresponding to each of the naturally occurring Trp residues (position −3 in the pro-segment, 8, 50, 72, and 108) in the N-terminal half of the protein. Structural analyses indicated that the conservative Phe-Trp substitutions did not perturb the conformation of the mutants with respect to the wild-type protein. Steady-state fluorescence studies indicated that all of the Trp residues exist in nonpolar environments that are highly protected from solvent in both the lipid-free and lipid-bound forms. Time-resolved lifetime and anisotropy studies indicated that the shape of the monomeric form of proapoA-I is a prolate ellipsoid with an axial ratio of about 6:1. In addition, the region surrounding Trp 108 appears to be more mobile than the rest of the protein in the lipid-free state. However, in rHDL particles, no significant domain motion was detected for any of the Trp residues. The results presented in this work are consistent with a model for monomeric lipid-free proapoA-I in which the N-terminal half of the molecule is organized into a bundle of helices.

Epidemiological and transgenic animal studies have convincingly demonstrated an important role for high-density lipoprotein (HDL)[1] and its major protein constituent, apolipoprotein (apo) A-I, in the protection against atherosclerosis in humans. As a result, substantial investigative effort has been directed toward understanding the molecular basis for this protective effect. Unfortunately, progress on this problem has been slow. A major hindrance has been the difficulty encountered in determining the structures of the apolipoprotein constituents of HDL. ApoA-I conformation is an important factor in all stages of reverse cholesterol transport (RCT), the process by which excess cellular cholesterol is returned to the liver for catabolism. Castro and Fielding (*1*) and others (*2, 3*) have proposed that lipid-poor forms of apoA-I that are conformationally distinct from the bulk of HDL-associated apoA-I may be particularly efficient in mobilizing excess peripheral cell cholesterol during the first step of RCT. This process has been termed apolipoprotein-mediated cholesterol efflux (see ref *4*) and represents a distinct pathway from the aqueous diffusion mechanism that is thought to be responsible for cellular cholesterol transfer to lipid-rich HDL particles (for reviews, see refs *5* and *6*). The conformation of apoA-I also regulates HDL particle maturation in plasma through effects on lecithin:cholesterol acyltransferase (LCAT) activity (*7, 8*). Recent evidence also suggests that the delivery of cholesterol for adrenal steroid hormone synthesis and liver bile acid synthesis via the SR−BI receptor may also be modulated by apoA-I (*9*). A molecular understanding of these important apoA-I-mediated processes requires knowledge of the conformation of lipid-poor apoA-I and the structural transitions that occur throughout the molecule as it binds lipids.

The approximate secondary structure of apoA-I has been inferred from the primary sequence (*10*) and from spectroscopic studies (see ref *11*). In general, the protein is arranged into 8 repeating, 22 amino acid amphipathic α-helical segments that are critical for lipid binding. Unfortunately, little information exists on the overall tertiary structure of apoA-I either in the lipid-free form or in HDL-like particles. Recently, Borhani et al. (*12*) reported an X-ray crystal structure for a lipid-free fragment of apoA-I that lacks the N-terminal 43 amino acids of the 243 amino acid, 28 kDa protein. The structure shows a homo-tetramer of highly α-helical apoA-I molecules arranged in a ring with the

† This work was supported by NIH Grant HL-16059 to A.J. and a postdoctoral fellowship from the American Heart Association, Illinois Affiliate, to W.S.D. The spectroscopic experiments were performed at the Laboratory for Fluorescence Dynamics (RR03155, supported by the NIH).

* Corresponding author. Phone: (217)333-0452. Fax: (217)333-8868. E-mail: a-jonas@uiuc.edu.

‡ Department of Biochemistry.

§ Present address: Department of Pathology and Laboratory Medicine, University of Cincinnati, 231 Bethesda Avenue, Cincinnati, OH 45267-0529.

|| Department of Physics.

[1] Abbreviations: a.a., amino acid residue; ACH, adrenocorticotropin hormone peptide; apoA-I, apolipoprotein A-I; BSA, bovine serum albumin; FC, free (unesterified) cholesterol; GdnHCl, guanidine hydrochloride; HDL, high-density lipoprotein; rHDL, reconstituted HDL; PAGGE, polyacrylamide gradient gel electrophoresis; PL, phospholipid; POPC, 1-palmitoyl-2-oleoylphosphatidylcholine; STB, standard Tris buffer; λ_{max}, wavelength of maximum fluorescence; WT, wild type.

10.1021/bi991428h CCC: $18.00
Published on Web 10/07/1999

monomers associating via the hydrophobic faces of the amphipathic α-helices. This important advance may shed light on how apoA-I self-associates and provide clues to the structure of the apolipoprotein in mature, spherical HDL particles. However, the applicability of this structure to monomeric forms of lipid-free apoA-I and to nascent, discoidal HDL particles is unclear. This truncated form of apoA-I has been shown by spectroscopic methods to exist in a substantially different conformation than native apoA-I when in the absence of lipids (*13*) and probably does not reflect the structure of monomeric, native apoA-I.

Studies from our laboratory have used deletion mutants of apoA-I to show that the soluble, monomeric form is organized into domains that roughly encompass the N- and C-terminal halves of the molecule (*14*). The N-terminal portion of apoA-I (approximately a.a. 1−139) was highly α-helical and primarily responsible for the stability of the protein in solution. On the other hand, the C-terminal portion (approximately a.a. 140−243) was relatively unstable. When in contact with lipid in reconstituted HDL particles, the N-terminal region underwent a rearrangement of α-helical segments without a major change in overall helicity. The C-terminus, however, became highly helical and was the major stabilizing domain. This model has been extended by Roberts et al. (*15*), who studied lipid-free apoA-I by limited proteolysis. They found that the C-terminal portion (in their case, approximately a.a. 190−243) of lipid-free apoA-I was highly susceptible to proteolysis, whereas the N-terminus was less exposed. An analysis of the cleavage patterns generated a model of lipid-free apoA-I consisting of a bundle of α-helices in the N-terminal region with an unorganized C-terminus. The notion of an organized N-terminal bundle of helices has also been supported by studies of chicken apoA-I (*16*) and for the related exchangeable apolipoprotein, apo E (*17*).

To further probe the structure and dynamics of the N-terminal region of lipid-free apoA-I, we studied the fluorescence properties of the five Trp residues in the N-terminal half of recombinant human proapoA-I (position −3 in the pro-segment, 8, 50, 72, and 108). The pro-form contains a hexapeptide on the N-terminus that is normally cleaved once the protein is secreted into the plasma. This form was used for these studies because of its high expression levels in bacterial cells vs the mature form (*18*) and because it exhibits structural and functional properties that are identical to the mature form isolated from human plasma (*19*). In the current work, each Trp residue was studied individually by replacing all the other naturally occurring Trp residues with nonfluorescent Phe. The results support the model for lipid-free, monomeric apoA-I in which the N-terminal Trp residues are closely packed in protein−protein contacts that are not maintained in the lipid-bound state in discoidal recombinant HDL (rHDL) particles.

EXPERIMENTAL PROCEDURES

Materials

Sodium cholate, bovine serum albumin (BSA), azurin, adrenocorticotropin hormone fragment 1−10 (SYSMEHFRWG), ampicillin, and 1-palmitoyl-2-oleoylphosphatidylcholine (POPC) were purchased from Sigma Chemical Co. (St. Louis, MO) (+99% grade). Kanamycin sulfate was purchased from CalBiochem (La Jolla, CA). The restriction enzymes, DH5α, and BL-21(DE3) competent *Escherichia coli* cells were obtained from GIBCO BRL (Gaithersburg, MA). The plasmid purifications were performed with either the gel purification kit or mini- and midi-prep kits from QiaGen (Valencia, CA). All other reagents were analytical grade.

Methods

*Construction of the Mutant cDNAs. Nco*I and *Hin*dIII restriction sites were engineered immediately upstream and downstream, respectively, of the coding sequence of the human proapoA-I cDNA (gift of Dr. J. I. Gordon, Washington University). The modified cDNA was subcloned into the multiple cloning site of the pBluescript SK (±) phagmid (Stratagene, La Jolla, CA). The five different single Trp mutants were generated by site-directed mutagenesis using either standard PCR-based techniques or the Quick-Change site-directed mutagenesis kit (Stratagene) using oligonucleotides produced at the University of Illinois Biotechnology center. The general strategy for the mutagenesis was as follows: each Trp residue was converted, one at a time, to Phe to yield a mutant that contained no Trp residues (W@ϕ). The nomenclature of W@X signifies that a Trp exists at position X and that all of the other positions that normally contain a Trp residue have been converted to Phe. W@108 was then produced by subcloning the wild type *Bsu*36−*Hin*dIII sequence into W@ϕ. Finally, W@ϕ was used as a template to put single Trp residues back into the sequence to generate W@−3, W@8, W@50, and W@72. The sequence of each construct was verified on an Applied Biotechnology System DNA sequencer.

Expression and Purification of proapoA-I Mutants. Each of the constructs created above were subcloned into the PET-28a(+) expression vector (Novagen, Madison, WI) using the *Nco*I and *Hin*dIII sites. The resulting plasmids were transfected into BL-21 (DE3) *E. coli* cells. The overexpression of the mutant proapoA-I was performed using freshly transfected cells grown in multiple 150 mL Luria-Bertani (LB) cultures supplemented with 30 μg/mL kanamycin at 37 °C. Protein synthesis was induced at an A_{600} of 0.7−0.8 by the addition of 1.5 mM IPTG followed by a 3-h, 37 °C incubation in a shaker rotating at 200 rpm. After harvesting, the cells were resuspended (15 mL/L of culture) in 10 mM Tris buffer, pH 8.0, containing 0.15 M NaCl (standard Tris buffer, STB) that had been freshly supplemented with 1.0 mM PMSF to prevent proteolysis. To monitor the levels of expression of the various mutants, a sample of the cell suspension was analyzed by SDS−PAGE, and the proapoA-I or mutant band was quantitated by laser densitometry (Pharmacia) and compared to a standard curve generated from purified proapoA-I run on the same gel. The suspension was passed three times through a French press cell (Aminco) and centrifuged at 18000*g* for 30 min at 4 °C. The supernate was applied to a Phenyl Sepharose column (Pharmacia, CL-4B) of 18−20 mL total bed volume at 25 °C at a flow rate of 1.0 mL/min. The column was washed with 200 mL of STB, and the protein was eluted with a linear gradient between STB and STB containing 60% ethylene glycol. The fractions containing the highest amounts of proapoA-I as estimated by SDS−PAGE were pooled, dialyzed against STB, and applied to a POROS 20 HQ anion exchange

column. The column was eluted with a gradient of STB + 3 M NaCl, pH 8.0, at 10 mL/min on a BioCAD workstation (Perseptive Biosystems, Framingham, MA), and optimal fractions were dialyzed into ammonium bicarbonate and stored lyophilized at −20 °C under nitrogen. W@8, W@50, and W@72 exhibited low expression levels and required additional purification on a Superdex 200 HR (Pharmacia, 10 × 30 mm) gel filtration column in STB containing 3 M guanidine hydrochloride (GdnHCl). The optimal protein fractions were dialyzed into ammonium bicarbonate and stored lyophilized.

Preparation and Characterization of rHDL Particles. Lyophilized proteins were solubilized in Tris buffer containing 6 M GdnHCl and then dialyzed into STB before use. All particles were reconstituted using the sodium cholate dialysis method described elsewhere (*20*). The initial molar ratios of PL to apolipoprotein were 100:1. The particles were isolated on a calibrated Superdex 200 HR (10 × 30 mm) gel filtration column eluted at 0.5 mL/min with Tris buffer. The hydrodynamic diameters of rHDL particles were estimated from the column elution volume and by native 8−25% polyacrylamide gradient gel electrophoresis (PAGGE) (Pharmacia) as described previously (*21*). Protein contents were determined by the Markwell/Lowry protein assay (*22*). Phospholipids were determined by the method of Sokoloff and Rothblat (*23*).

Circular Dichroism (CD) and Isothermal Denaturation Studies. The average α-helical contents of apoA-I and the mutants were determined by CD spectroscopy using a Jasco J-720 spectropolarimeter at 222 nm. Spectra were measured from 190 to 250 nm at 25 °C in a 0.1-cm quartz cuvette. Sample concentrations of 0.05−0.1 mg/mL (in 20 mM phosphate buffer, pH 7.8, with 10 μM NaCl) were used so that all apolipoproteins were monomeric (*14*). The α-helix contents of the proteins after 72-h incubations with increasing concentrations of GdnHCl at 4 °C were used to obtain the free energy of unfolding of apoA-I as proposed by Tanford and Aune (*24*) and modified by Sparks et al. (*25*).

Fluorescence Spectroscopy. The concentration of protein was 0.05−0.1 mg/mL (in 20 mM phosphate buffer, pH 7.8, with 10 μM NaCl) for all fluorescence studies. The wavelength of maximum fluorescence (λ_{max}) of the Trp residues was determined from uncorrected spectra on a Perkin-Elmer MPF-66 fluorescence spectrophotometer using 4 nm excitation and emission band-passes. The samples were excited at 295 nm to avoid tyrosine fluorescence. The emission was scanned from 305 to 450 nm at 25 °C. Fluorescence quenching experiments were carried out using increasing concentrations of acrylamide (0−0.2 M). After correction for buffer effects, the quenching parameters were calculated using a Stern−Volmer analysis (*26*, *14*).

Tryptophan lifetime measurements were performed using a multifrequency cross-correlation phase and modulation fluorometer (ISS Inc.) at an excitation wavelength of 295 nm. The light source was a rhodamine dye laser synchronously pumped by a mode-locked Nd:YAG laser (Coherent). The output of the dye laser was frequency doubled to 295 nm and passed through a U 325 (HOYA) band-pass filter to remove any 590 nm light. The emission was collected through a long pass filter (WG 320, Schott) and a U-330 band-pass filter to remove scattered light. The Trp lifetimes were observed under magic angle conditions in which the excitation beam was polarized normal to the laboratory plane (0°) and the emission polarizer was set to 54.7°. *p*-Terphenyl in absolute ethanol (τ = 1.05 ns) was used as a lifetime reference. The phase and modulation data were collected across a harmonic range of 3−300 MHz. The data were analyzed using Globals Unlimited software (LFD, Urbana, IL) for multiple lifetime components with a constant error of the modulation and phase data fixed at 0.004 and 0.2, respectively. Time-resolved anisotropy measurements were made on the same machine under the same conditions. The polarization data was analyzed for two rotational correlation times, one for fast local motion and a second for slower global motion (*27*, *28*).

RESULTS

Expression of the Mutant proapoA-I. Upon treatment of the bacterial cells with IPTG, 90% of the total expressed proapoA-I was found in the soluble fraction after cell lysis. We observed mutant-specific differences in the protein expression levels. WT proapoA-I and W@-3 exhibited the highest expression efficiencies of approximately 18−19 mg of protein/L of culture. The W@108 levels were somewhat lower (13 mg/L), but the remaining mutants were expressed much less efficiently (3−5 mg/L). The reason for these differences in expression is not clear, but it appears that the integrity of the pro-segment, which was not affected in WT and W@-3, is an important determinant in expression efficiency in this system. All of the mutants exhibited similar elution profiles to the WT on the hydrophobic interaction and anion-exchange columns, indicating that the sequence manipulations had minimal effects on the overall hydrophobicity and ionization state of the variants. An SDS−PAGE analysis of the purified mutants showed that all of the mutants migrated similarly to the WT proapoA-I with a calculated MW of about 28 kDa (data not shown). All proteins were determined to be at least 95% pure by laser densitometry.

Nonfluorescent Characterization of the Lipid-Free and Lipid-Bound Proteins. The use of the Trp mutants in fluorescence studies depends on the assumption that the Phe to Trp replacements did not perturb the structure and function of the WT proapoA-I. All of the mutants were capable of forming rHDL particles of similar size and composition as WT proapoA-I. All rHDL particles were between 9.6 and 9.8 nm in diameter by native PAGE analysis (not shown). The average molar phospholipid-to-protein ratios were 91:1, 87:1, 70:1, 75:1, 70:1, and 84:1 for WT, W@−3, W@8, W@50, W@72, and W@108 respectively (average SD was ±20). Complexes of this size are known to contain two molecules of apoA-I per complex (*19*, *29*). Since WT apoA-I is known to self-associate at concentrations in excess of 0.1 mg/mL, we measured the abilities of the mutants to form oligomers in solution by cross-linking with the divalent cross-linker BS_3. Figure 1A shows that all mutants and WT formed oligomers ranging from dimers to pentamers in approximately similar distributions when cross-linked at 1.0 mg/mL. No cross-linked proteins were observed at 0.1 mg/mL for any mutant (Figure 1B), indicating that they are monomeric below this concentration.

Far-UV circular dichroism was used to estimate the average secondary structures of the lipid-free and rHDL-

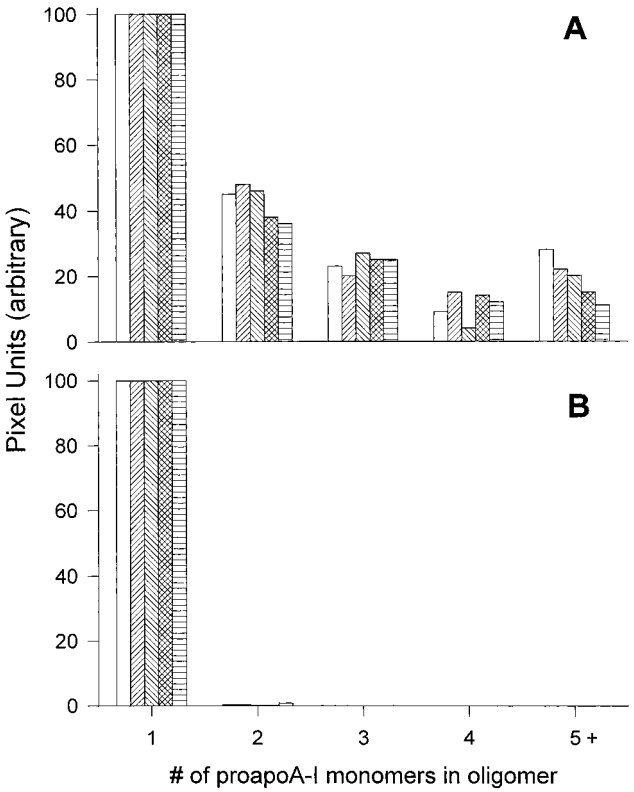

FIGURE 1: BS_3 cross-linking study on the self-association properties of the proapoA-I variants at low and high concentrations. All of the proapoA-I samples used in this study were cross-linked at 1.0 (panel A) and 0.1 mg/mL (panel B). After 3 h of incubation with the cross-linker at room temperature, the samples were lyophilized, resuspended in SDS running buffer, and electrophoresed on 8−25% SDS gels. The gels were then stained with Coomassie blue and scanned into a computer. Jandel SigmaScan software was used to quantify the pixels associated with each band. The peak pixel intensity in each lane was assigned a value of 100 (monomer), and the other values are scaled as a percentage.

bound variants. The spectra were similar for all of the lipid-free mutants and WT (Figure 2A,B). In the lipid-bound state, the magnitude of the minima at 208 and 222 nm were increased consistent with an increase in helical content, and no major differences were observed between the variants and WT. The calculated α-helical contents expressed as the percentage of total amino acids are shown in Table 1. All mutants exhibited similar α-helix contents that were within experimental error of the average of 54% for the lipid-free proteins and 80% for the rHDL particles. We have reported similar values for human plasma apoA-I (*30*) and for recombinant proapoA-I (*19*).

Table 1 also shows the results of a particle charge analysis of the variants in both forms. Since the Phe to Trp substitutions do not affect charged residues, the similar values for all of the mutants indicate that the ionization states of charged amino acids were not perturbed, suggesting that the overall conformation of the mutants was not significantly different than WT (*31*).

To determine the effects of the substitutions on the stability of the protein, far-UV CD was used to monitor the stability of the mutants in the presence of the chemical denaturant GdnHCl. Table 2 shows that WT proapoA-I exhibits a $\Delta G°$ of about 2.5 kcal/mol, which is similar to previously reported values (*19*). The lipid-free mutants, however, exhibited a $\Delta G°$ that averaged about 1.4 kcal/mol, indicating that the Trp to Phe substitutions decreased the stability of WT proapoA-I. In a separate work, we have used mutants that have only 2 of the 5 Trp residues replaced to show that this effect is dependent on the number of Trp residues replaced (*32*). In the case of the lipid-bound proteins, however, the apparent $\Delta G°$ values of all the variants were similar to previously reported values of 2.9 kcal/mol for human plasma apoA-I (*33*) and WT recombinant proapoA-I (*19*).

Steady-State Fluorescence Spectroscopy of the Lipid-Free and Lipid-Bound Proteins. We proceeded to study, for the first time, the fluorescence properties of the individual Trp residues in proapoA-I. This study included two control proteins that each had a single Trp residue present in the extremes of solvent exposure. The first is a 10 a.a. peptide from adrenocorticotropin hormone (ACH) that does not have a defined structure in aqueous buffer. This is a control for the upper limit of solvent exposure for a peptide-constrained Trp residue. The second protein, azurin, is an iron-containing, 48 kDa protein that contains a single Trp (position 48) in a completely sequestered environment within the core of the protein (*34*).

The wavelength of maximum fluorescence (λ_{max}) gives an indication of the polarity of the Trp environment. Burstein et al. (*35*) have classified Trp residues into λ_{max} ranges as follows: class I (330−332 nm), buried in nonpolar regions of protein; class II (340−342), surface but limited solvent contact; class III (350−352), completely solvent exposed. Table 2 shows that the highly exposed Trp in ACH peptide exhibited a red-shifted λ_{max} of 354 nm. Azurin, on the other hand, exhibited a blue-shifted value of 308 nm. This value is blue-shifted from that of typical class I Trp residues because of its proximity to a copper binding region in the protein (*34*). In the case of the lipid-free apolipoproteins, WT proapoA-I exhibited a λ_{max} of 336 nm that represents the average environment of all five Trp residues in the protein. Of the variants, W@−3 and W@50 were red-shifted about 2 nm, indicating that Trp −3 and 50 exist in a slightly more polar environment than average. W@108 was blue-shifted relative to WT, indicating a highly nonpolar environment for Trp 108. The λ_{max} for Trp 8 and Trp 72 were near the average. Trp residues −3, 8, 50, and 72 all fell between class I and II Trp residues, indicating that they are located in minimally solvent exposed, protein-protected environments in the lipid-free state. Trp 108 fell in class I, suggesting that it is completely protected by protein. In rHDL particles, each of the individual Trp residues in the mutants experienced a blue-shift ranging from 1 to 6 nm, indicating a transition to a more hydrophobic state. The fact that all Trp residues underwent a blue shift suggests that they did so through some form of a lipid interaction. Studies of single Trp proteins that are known to bind lipid, such as mellittin (*36*) and a nisin mutant (*37*), have shown that the λ_{max} of Trp residues exposed to lipid are 331 and 332 nm, respectively.

The fluorescence spectra of WT proapoA-I and the variants in the lipid-free form and in rHDL are shown in Figure 3, panels A and B, respectively. The null mutant W@ϕ (not shown) exhibited minimal background fluorescence as expected for a Tyr-only containing protein at an excitation wavelength of 295 nm. In the case of the lipid-free mutants, the intensities of the individual Trp emissions from the mutants can be summed up to a much higher intensity than was observed for the WT protein. Thus, the quantum yield

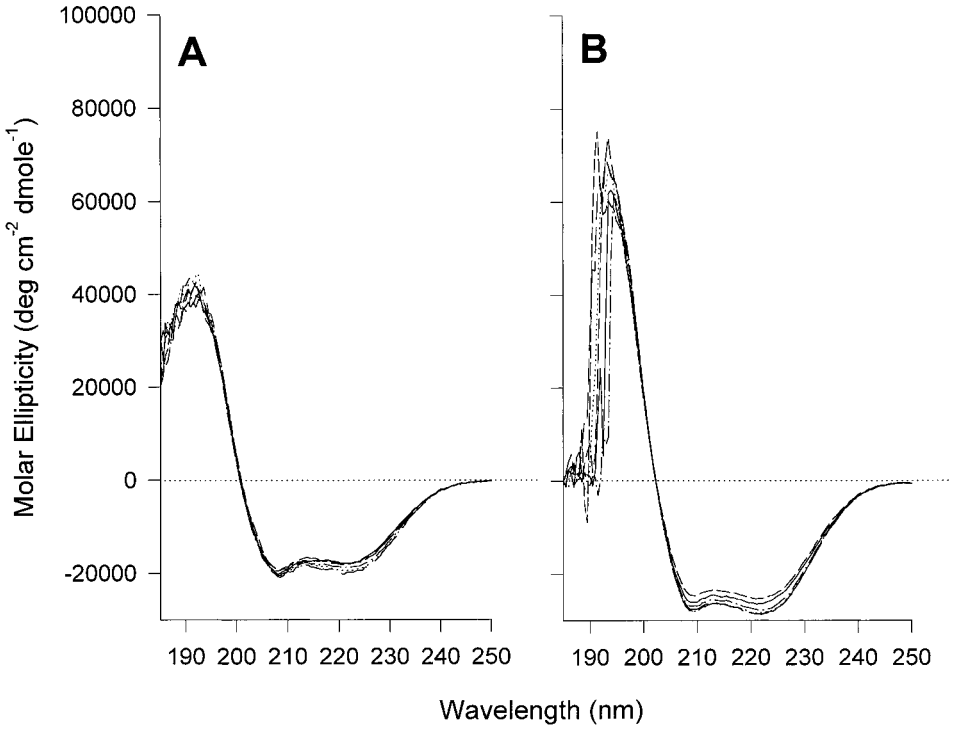

FIGURE 2: Far-UV circular dichroism spectra of the mutants of proapoA-I in the lipid-free state (panel A) and in 96 Å discoidal rHDL particles (panel B). The spectra were collected in 20 mM phosphate buffer, pH 7.8, with 10 μM NaCl at 25 °C at a concentration of 0.1 mg/mL for all samples. All five of the Trp mutants are shown along with the spectrum for the wild-type protein in both panels. Due to the large number of samples and the high degree of spectral overlap, no attempt was made to distinguish between each individual Trp mutant in this figure.

Table 1: Conformation and Stability Properties of the WT proapoA-I and the Single Trp Mutants in the Lipid-Free and Lipid-Bound Forms

	α-helix content[a]		valence (±0.1 e)[b]		$\Delta G_D°$ (±0.3 kcal/mol apoA-I)[c]	
	lipid-free (±6%)	rHDL (±7%)	lipid-free	rHDL	lipid-free	rHDL[d]
WT proapoA-I	56	78	−3.0	−7.3	2.5	3.2
proapoA-I W@−3	57	84	−3.0	−7.4	1.1	2.9
proapoA-I W@8	54	80	−3.0	−7.4	1.6	3.2
proapoA-I W@50	52	73	−2.9	−7.5	1.5	3.5
proapoA-I W@72	51	86	−3.0	ND[e]	1.3	ND
proapoA-I W@108	56	84	−2.9	−7.5	1.3	3.3

[a] α-Helical contents determined from the molar ellipticity at 222 nm at 25 °C as calculated according to Chen et al. (*50*). Each value represents the average of at least three observations. The reported experimental error is an average SD derived from all samples in a given set. [b] The net number of negative charges per molecule or particle as determined at pH 8.6 at 25 °C from migration in 0.5% agarose gels. The experimental error of ±0.1e has been reported for this method (*31*) previously. [c] Standard change in free energy of denaturation of the α-helical segments monitored by circular dichroism at 222 nm (±1 average SD) in response to increasing concentrations of GdnHCl. [d] The derivation of ΔG values depend on the assumption that the denaturation reaction is reversible. Since the denaturation of rHDL complexes has a reversible and a nonreversible component, the ΔG values derived for the rHDL complexes were calculated according to the correction procedure proposed by Sparks et al. (*25*) and should be considered "apparent" values. [e] ND, not determined.

of the five Trp residues present together was lower than when each was present separately. This phenomenon was not observed in the case of the lipid-bound proteins (Figure 3B).

To more precisely determine the relative exposure of each residue to solvent, acrylamide quenching studies were performed (Table 2, Figure 4). Trp residues that are exposed to solvent collide with soluble acrylamide resulting in a nonradiative relaxation of the excited state, which is measured as decreased fluorescence intensity. The K_{sv} term (the slope of the lines in Figure 4) reflects the relative accessibility of the Trp residues. Low K_{sv} indicate nonsolvated environments; high values indicate high solvent exposure. The Trp in azurin was not quenched by acrylamide and gave a low K_{sv} as expected. The highly exposed Trp in ACH peptide was easily quenched and gave a K_{sv} of about 18 M^{-1}. In general, the lipid-free proapoA-I mutants exhibited protected Trp environments giving K_{sv} values closer to that of azurin than that of the ACH peptide. W@50 and W@-3, in agreement with the λ_{max} data, appeared to have the most exposed Trp residues of the lipid-free proteins. Once bound to lipid, the Trp residues in all of the mutants exhibited a decreased K_{sv}, indicating a change to a more solvent-protected environment. The similarity of the K_{sv} values for the rHDL particles strongly suggests that all of the Trp residues are protected from solvent as a result of a direct interaction with lipid. It is worth noting that all of the plots in Figure 4 were linear. This may indicate that there is little conformational heterogeneity within the samples in both the lipid-free and lipid-bound forms (*26*).

Time-Resolved Fluorescence Spectroscopy of the Lipid-Free and Lipid-Bound Proteins. To obtain information on the rotational motions of the Trp residues within proapoA-

Table 2: Steady-State Fluorescence Parameters of WT proapoA-I and the Single Trp Mutants in the Lipid-Free and Lipid-Bound States

	λ_{max}[a] (±2 nm)		K_{sv}[b] (±1.0 M^{-1})	
	lipid-free	rHDL (96 Å)	lipid-free	rHDL (96 Å)
WT proapoA-I	336	335	4.0	3.3
proapoA-I W@−3	338	332	7.2	3.0
proapoA-I W@8	335	332	7.0	2.7
proapoA-I W@50	338	336	4.7	2.7
proapoA-I W@72	335	330	5.7	ND[c]
proapoA-I W@108	332	331	3.5	2.2
azurin	308		1.0	
ACH-peptide	354		18.6	

[a] From uncorrected spectra at 25 °C. The experimental error of ±2 nm is from an average sample standard deviation based on at least six observations. [b] Stern−Volmer constant indicating relative exposure of quencheable fluorescence to the quenching agent acrylamide. The experimental error of ±1.0 M^{-1} is from an average sample standard deviation based on at least three observations. [c] ND, not determined.

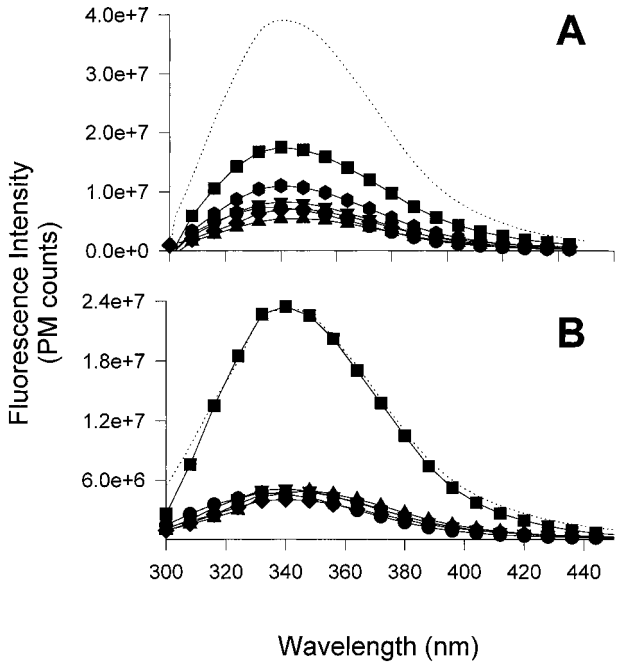

FIGURE 3: Steady-state fluorescence spectra of the mutants of proapoA-I in the lipid-free state (panel A) and in 96 Å discoidal rHDL particles (panel B). The spectra were collected in 20 mM phosphate buffer, pH 7.8, with 10 μM NaCl at 25 °C at a concentration of 0.1 mg/mL for all samples. The excitation wavelength was 295 nm. In both panels: wild-type proapoA-I (■), proapoA-I W@-3 (▲), proapoA-I W@8 (▼), proapoA-I W@50 (♦), proapoA-I W@72 (⬢), and proapoA-I W@108 (●). The arithmetic sum of all of the single Trp mutants is shown in each panel as a dotted line.

I, we measured the fluorescent lifetimes and the time-resolved anisotropies for each mutant. The phase and modulation data for each of the mutants as a function of excitation frequency were fitted to discrete exponential decay models. The best fits to the data were determined by comparing the reduced χ^2 values and using a correlated error analysis as previously described (*38*). Table 3 shows that most of the lifetimes of the proteins in this study were best fit to three discrete exponential decays. The exception was the ACH peptide, which fit to a double exponential decay. The presence of multiple decays for proteins containing a single Trp residue is a common observation (*39*, *40*, *27*),

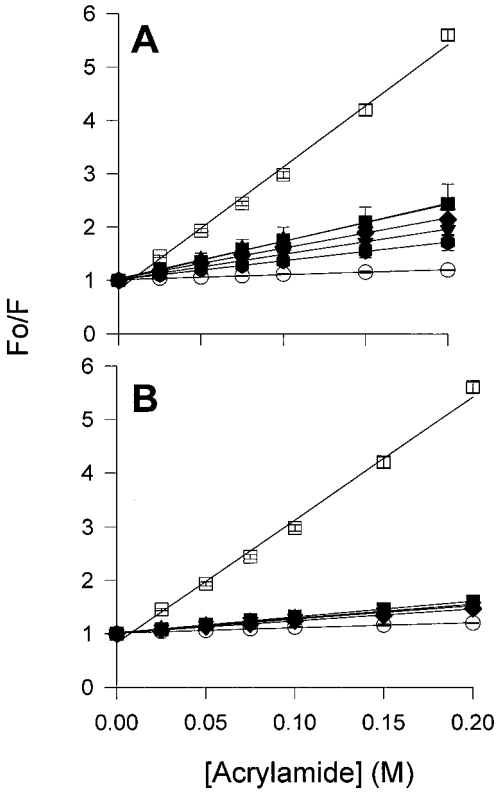

FIGURE 4: Steady-state Stern−Volmer plots of the mutants of proapoA-I in the lipid-free state (panel A) and in 96 Å discoidal rHDL particles (panel B). The spectral moments from the spectra (scanned from 305 to 375 nm) of the Trp mutants were used to determine the ratio of F_o (intensity in the absence of acrylamide) to F (intensity in the presence of the indicated concentration of acrylamide). The spectra were collected under same conditions as those stated in Figure 3. The excitation wavelength was 295 nm. In both panels: wild-type proapoA-I (■), proapoA-I W@-3 (▲), proapoA-I W@8 (▼), proapoA-I W@50 (♦), proapoA-I W@72 (⬢), proapoA-I W@108 (●), ACH peptide (□), and azurin (○).

but the cause for such heterogeneity is a controversial topic in photophysics. The lifetimes were generally distributed between a long component of approximately 5−7 ns, a short 2−4 ns component, and a subnanosecond component that made up only a small percentage of the emission for most of the proteins. The ACH peptide lacked the long component, suggesting that stable interactions with other protein regions or lipid may be required for the presence of a long component. W@72 had a higher fraction of its emission associated with the long lifetime. This resulted in an average lifetime that stood out as longer than the rest of the mutants and was in agreement with its higher quantum yield as seen in Figure 3A. The transition to the lipid-bound state did not have any systematic effect on the lifetime distributions between the various mutants. However, the average lifetimes tended to be slightly longer for the rHDL particles.

We proceeded to measure the rotational correlation times for each mutant. The data were fit to a model that contains two rotational correlation times, a local correlation time (ϕ_2) and a global correlation time (ϕ_1). The local value represents the local motion of the Trp residue at its point of attachment in the polypeptide. The global time can represent the tumbling of a rigidly organized protein, or it can represent a weighted average of the tumbling of a protein and the movement of smaller, flexible domain within the protein. The f_1 term represents the fractional contribution of this

Table 3: Fluorescence Lifetime Parameters of the Single Trp Mutants in the Lipid-Free and Lipid-Bound States

	lifetimes (ns)[a]			fractional contributions				
	τ_1 (±6%)	τ_2 (±11%)	τ_3 (±17%)	f_1 (±12%)	f_2 (±13%)	f_3 (±18%)	av lifetime (ns)[b]	χ^2 [c]
WT proapoA-I								
lipid free	5.3	2.3	0.7	0.32	0.56	0.12	3.1	0.3
rHDL	5.9	2.1	0.4	0.60	0.35	0.05	4.3	1.0
proapoA-I W@−3								
lipid free	5.7	2.3	0.4	0.30	0.56	0.15	3.0	1.0
rHDL	7.3	2.7	0.6	0.42	0.49	0.09	4.4	1.2
proapoA-I W@8								
lipid free	5.9	2.8	0.5	0.40	0.53	0.08	3.8	0.9
rHDL	7.8	3.7	0.9	0.28	0.65	0.08	4.6	0.5
proapoA-I W@50								
lipid free	6.5	2.7	0.8	0.37	0.51	0.13	3.8	0.6
rHDL	6.7	2.8	0.7	0.48	0.44	0.09	4.5	0.6
proapoA-I W@72								
lipid free	6.3	2.1	0.3	0.79	0.17	0.04	5.3	0.8
rHDL	7.3	3.3	0.7	0.58	0.36	0.06	5.4	1.1
proapoA-I W@108								
lipid free	5.1	1.8	0.2	0.46	0.40	0.15	3.1	0.8
rHDL	10.8	3.4	0.8	0.11	0.76	0.13	3.9	1.5
azurin	4.2	1.1	0.2	0.67	0.10	0.24	2.9	2.9
ACH-peptide[d]		3.3	1.0		0.89	0.12	3.0	0.5

[a] Data were taken at 20 °C in 20 mM phosphate buffer at pH 7.8. The experimental errors represent average standard deviations as a percentage of the mean derived from measurements of three independent samples. [b] The average lifetime is calculated from the three lifetime fractional components by the formula: $(\tau_1 f_1) + (\tau_2 f_2) + (\tau_3 f_3)$ where τ_x is the lifetime of a given fractional component and f_x is the fractional contribution of that component. [c] χ^2 is the reduced chi-squared value for the fit assuming errors of 0.2° and 0.004 for phase and modulation data, respectively. [d] The data from the ACH peptide samples were best fit to a two-component model.

Table 4: Time-Resolved Anisotropy Parameters of the Single Trp Mutants in the Lipid-Free and Lipid-Bound States

	rotational correlation times (ns)[a]		fractional contributions	
	ϕ_1 (±10%)	ϕ_2 (±10%)	f_1 (±3%)	χ^2 [b]
WT proapoA-I				
lipid free	22.5	0.18	0.72	0.6
rHDL	25.1	0.20	0.61	2.4
proapoA-I W@−3				
lipid free	59.2	0.44	0.27	2.3
rHDL	33.1	0.30	0.51	2.0
proapoA-I W@8				
lipid free	23.2	0.24	0.64	2.1
rHDL	22.6	0.21	0.62	1.3
proapoA-I W@50				
lipid free	18.8	0.16	0.61	1.4
rHDL	24.0	0.15	0.53	2.8
proapoA-I W@72				
lipid free	28.2	0.21	0.68	1.1
rHDL	52.0	0.20	0.58	1.7
proapoA-I W@108				
lipid free	6.7	0.19	0.46	1.1
rHDL	31.5	0.23	0.58	0.6
ACH-peptide[c]	1.2	0.15	0.85	0.6

[a] The experimental conditions were the same as in Table 3. The experimental errors represent average standard deviations as a percentage of the mean derived from the spectra of three independent samples. ϕ_1 represents the "global " motion of the protein whereas ϕ_2 represents "local" motion of the Trp residue. A limiting anisotropy of 0.30 was used for all samples (*39*). [b] χ^2 is the reduced chi-squared value for the fit assuming errors of 0.2° and 0.004 for phase and modulation data, respectively. [c] Data were taken for the azurin sample, but the computer fits to the data generated impossibly large numbers for the global correlation times with high χ^2 values. The reason for our inability to fit the data for azurin was not clear, but it may be due to the proximity of the Trp residue to the copper group within the protein.

motion to the overall decay. Table 4 lists the results for both the lipid-free and lipid-bound forms of the mutants. Taking the case of the lipid-free proteins first, the global correlation time ranged from 19 to 59 ns for W@−3, 8, 50, 72, and WT. Interestingly, the global correlation time for the mutant containing the Trp at position 108 was significantly shorter than the others. This suggests that the region surrounding this residue may undergo substantial segmental motions relative to the rest of the protein. The global correlation time measured for the WT protein was similar to the average value of all of the individual correlation times determined from each Trp residue. In terms of the local motions, all of the lipid-free proteins exhibited generally similar ϕ_2 values of 0.16−0.34 ns. These were comparable to those of the ACH peptide as well as other previously studied apolipoproteins (*37*), indicating relatively fast local motions for all of the Trp residues. The global correlation times for the lipid-bound forms of the proteins ranged widely from 23 to 52 ns. Finally, comparison of the local motions for the rHDL complexes revealed no major differences between mutants or between the lipid-free and lipid-bound forms.

DISCUSSION

As presented above, the lipid-free, monomeric form of apoA-I appears to exhibit a general domain organization. The α-helical segments in the N-terminal half of the protein are thought to be arranged in a bundle (*14*, *15*), whereas the C-terminal residues appear to be less organized. The current study tested this hypothesis using site-directed mutagenesis to examine each of the five individual Trp residues in the N-terminal half of recombinant proapoA-I. The major results from this study are discussed below within the context of this model.

Effect of Multiple Trp to Phe Substitutions on the Structure of ApoA-I. The observation that the four amino acid substitutions had little structural consequences was somewhat surprising since the Trp residues that occur in the mature protein are well-conserved among nonavian species from humans to mice (*41*). However, numerous naturally occurring point mutants and several point mutagenesis studies have

shown that single residue substitutions in a variety of sites in apoA-I have relatively few clinical or structural consequences (*42* and reviewed in ref *11*). Thus, it appears that, by virtue of its structural plasticity, apoA-I can accommodate a variety of conservative mutations. On the other hand, we were able to measure a change in the stability of the structure or at least the α-helical component of the structure in response to the Phe substitutions. Thus, Trp residues (and, hence, the N-terminal half of the molecule) appears to play a role in the marginal stability of the lipid-free protein.

Environments of the Individual Trp Residues—the Lipid-Free State. The λ_{max} and acrylamide quenching data show that all Trp residues are in hydrophobic environments in the lipid-free form. Since the sample contains only monomeric protein, this observation must be due to the sequestration of each Trp residue within a folded protein structure. The exhaustive sequence analysis performed by Nolte and Atkinson (*10*) predicts that Trp 72 and Trp 108 are present in α-helical regions. Trp 50 and Trp 8 are predicted to be in either random coil or β-sheet regions. In contrast, the model of Roberts et al. (*15*), based on exposed proteolytic sites, places all of the mature protein Trp residues in putative α-helical regions. These authors proposed that a number of these segments are arranged such that their hydrophobic faces interact to form a hydrophobic core to prevent solvation of the nonpolar faces. Such a four-helix bundle would fit well with the λ_{max} and acrylamide quenching data shown in Table 2. For example, an examination of helical wheel diagrams for each of the putative helical domains shows that Trp 50 is located at the interface between the polar and nonpolar face of helix 1 [helices numbered according to Roberts et al. (*15*)]. Trp 50 exhibited λ_{max} and K_{sv} values that suggested a slightly higher solvent exposure than most of the other Trp residues. The location of this residue at the interface can account for this observation. In contrast, Trp 108 is located directly in the center of the nonpolar face of helix 3. This residue was the least solvent exposed, consistent with its location deep within a hydrophobic core created by a α-helical bundle. In addition, the fluorescence intensity data (Figure 2) suggests that at least two of the Trp residues undergo energy transfer when present in the same protein. Since fluorescence energy transfer is distance-dependent, this indicates that the residues should be in close proximity, within approximately ∼5 Å (*43*). Further studies that use two and three Trp-containing proteins, analyzed by detailed anisotropy experiments, will be required to determine which of these Trp residues are close together.

Environments of the Individual Trp Residues—the Lipid-Bound State. Each of the Trp residues showed a blue fluorescence spectral shift when reconstituted into rHDL particles and had a decrease in the degree of exposure to acrylamide vs the lipid-free form. Such a transition must result from either protein−lipid contacts or to modified protein−protein contacts that further protect the Trp from solvent. Since Trp 72 and Trp 108 are located on the nonpolar face of putative helices 2 and 3, respectively, it is likely that these residues become buried within the lipid milieu. Trp 50 may experience a mixed lipid and protein environment. The fact that Trp −3 and Trp 8 also undergo a similar blue shift and decrease in solvent exposure is highly suggestive, but not conclusive, that these residues also associate with lipid. Future experiments that utilize phospholipids containing spin-labeled fatty acid side chains will be useful for determining the positions of Trp residues with respect to the bilayer surface.

Rotational Characteristics of apoA-I in the Lipid-Free and Lipid-Bound Forms. The global rotational correlation times (Table 4) measured for WT, Trp −3, 8, 50, and 72 in the lipid-free protein varied between 19 and 59 ns. The predicted rotational correlation time for a hydrated sphere of the size of monomeric apoA-I is about 12 ns as calculated by the Stokes−Einstein relationship for a rigid, spherical body (see ref *44*). Since the mutants and WT are nearly 100% monomeric at the concentration used for the fluorescence measurements (0.1 mg/mL) (Figure 1), the most likely explanation for the observed global correlation times is that the monomers deviate substantially from a spherical shape. This conclusion is consistent with the studies of Barbeau et al. (*46*). These investigators utilized analytical ultracentrifugation, viscometric, and fluorescence studies to demonstrate that apoA-I is a prolate ellipsoid with an axial ratio of about 5.5:1. If apoA-I has a prolate ellipsoid shape, there will be three distinct rotational correlation times associated with the global tumbling of the protein. Given this axial ratio and a molecular weight of 28 kDa, the rotational correlation times can be estimated as 12, 31, and 64 ns (*28, 27, 44, 47*). In most cases, only a single global rotational correlation time can be resolved experimentally (*48*). Hence, the single correlation time represents a weighted mean of the tumbling motions present and will depend on the orientation of the tryptophan with respect to the rotational axes of the protein. The results for the global correlation times in Table 4 are entirely consistent with the prolate model of Barbeau and co-workers. Furthermore, the fact that the single tryptophan mutants showed a wide range of rotational correlation times and that the longest time was near the calculated maximum value (64 ns) strongly supports a prolate over an oblate shape for apoA-I (*28, 47*). In the context of a prolate ellipsoid of this size, the extremely short global correlation time for the Trp at position 108 is striking. Since the observed value is shorter than even the theoretical value for a sphere, we are forced to conclude that the Trp in this region experiences significant segmental motions. The observed value may be an average consisting of the domain motion and global tumbling components. The observation of a high degree of mobility for the region surrounding Trp 108 was surprising given that this Trp appears to be the most highly protected of all of the Trp residues studied. Although the exact size of the mobile domain cannot be directly determined from these studies, it must be assumed that the region is large enough so that Trp 108 remains buried within the flexible protein region. It is interesting to note that Trp 108 is located within a putative "hinge domain" that comprises helices 3 and 4. This region has been implicated in the adaptation of apoA-I to HDL complexes of various sizes (*49*).

In terms of the rHDL complexes, the theoretical considerations are changed by the large size of the complexes. Each rHDL particle contains two molecules of proapoA-I and about 190 molecules of POPC, a combined molecular weight of about 200 kDa. In addition, the discoidal shape of the particle further slows the overall rotation. Assuming an axial ratio of about 3/1, a density of 1.112 g/mL, and 0.3 g of H_2O/g of complex, we estimate that an oblate ellipsoid (disk) has a theoretical correlation time of about 166 ns. Therefore,

during the average lifetime of lipid-bound Trp (4−5 ns), the disk has moved through only a small percentage of its rotation, and the global motions represent a small component of the ϕ_1 values listed in Table 4. It follows that the values in Table 4 primarily reflect domain motions occurring in the disk. The values measured for each Trp residue are generally similar to those found for the lipid-free proteins; i.e., we did not detect domain motions that were smaller than an entire molecule of apoA-I. Thus, we conclude that the regions containing these Trp residues in apoA-I are relatively stationary on the lipid disk and do not move independently of the rest of apoA-I. The origin of the domain motions measured likely come from motions within the disk, perhaps by oscillations of entire apoA-I molecules on the disk edge. It should be noted that this observation holds only for a 96 Å disk that is predicted to have all eight of the amphipathic helical segments associated with lipid (*29*). The data do not preclude the possibility that the mobility of any of these Trp residues could change when the size of the disk or the conformation of apoA-I is changed.

Finally, while this study primarily focused on the Trp residues in the N-terminal region and the lipid-free state of proapoA-I, we feel that this mutagenesis strategy will be extremely useful for probing the structure of this protein in rHDL particles of various sizes and shapes. In addition, the insertion of Trp residues in the C-terminal half of the molecule should offer new information on the dynamics and functional importance of this region as well.

ACKNOWLEDGMENT

We thank Nick Maiorano for his expert technical assistance.

REFERENCES

1. Castro, G. R., and Fielding, C. J. (1988) *Biochemistry 27*, 25.
2. Li, Q., Tsujita, M., and Yokoyama, S. (1997) *Biochemistry 36*, 12045.
3. Mendez, A. J. (1997) *J. Lipid Res. 38*, 1807.
4. Yokoyama, S. (1998) *Biochim. Biophys. Acta 1392*, 1.
5. Johnson, W. J., Mahlberg, F. H., Rothblat, G. H., and Phillips, M. C. (1991) *Biochim. Biophys. Acta 1085*, 273.
6. Rothblat, G. H., Llera-Moya, M., Atger, V., Kelner-Weibel, G., Williams, D. L., and Phillips, M. C. (1999) *J. Lipid Res. 40*, 781.
7. Glomset, J. A. (1968) *J. Lipid Res. 9*, 155.
8. Jonas, A., Kezdy, K. E., and Wald, J. H. (1989) *J. Biol. Chem. 264*, 4818.
9. Rigotti, A., Trigatti, B., Babitt, J., Penman, M., Xu, S., and Krieger, M. (1997) *Curr. Opin. Lipidol. 8*, 181.
10. Nolte, R. T., and Atkinson, D. (1992) *Biophys. J. 63*, 1221.
11. Brouillette, C. G., and Anantharamaiah, G. M. (1995) *Biochim. Biophys. Acta 1256*, 103.
12. Borhani, D. W., Rogers, D. P., Engler, J. A., and Brouillette, C. G. (1997) *Proc. Natl. Acad. Sci. U.S.A. 94*, 12291.
13. Rogers, D. P., Brouillette, C. G., Engler, J. A., Tendian, S. W., Roberts, L., Mishra, V. K., Anantharamaiah, G. M., Lund-Katz, S., Phillips, M. C., and Ray, M. J. (1997) *Biochemistry 36*, 288.
14. Davidson, W. S., Hazlett, T., Mantulin, W. W., and Jonas, A. (1996) *Proc. Natl. Acad. Sci. U.S.A. 93*, 13605.
15. Roberts, L. M., Ray, M. J., Shih, T. W., Hayden, E., Reader, M. M., and Brouillette, C. G. (1997) *Biochemistry 36*, 7615.
16. Kiss, R. S., Kay, C. M., and Ryan, R. O. (1999) *Biochemistry 38*, 4327.
17. Wilson, C., Wardell, M. R., Weisgraber, K. H., Mahley, R. W., and Agard, D. A. (1991) *Science 252*, 1817.
18. Moguilevsky, N., Roobol, C., Loriau, R., Guillaume, J. P., Jacobs, P., Cravador, A., Herzog, A., Brouwers, L., Scarso, A., and Gilles, P. (1989) *DNA 8*, 429.
19. McGuire, K. A., Davidson, W. S., and Jonas, A. (1996) *J. Lipid Res. 37*, 1519.
20. Jonas, A. (1986) *Methods Enzymol. 128*, 553.
21. Davidson, W. S., Rodrigueza, W. V., Lund-Katz, S., Johnson, W. J., Rothblat, G. H., and Phillips, M. C. (1995) *J. Biol. Chem. 270*, 17106.
22. Markwell, M. A., Haas, S. M., Bieber, L. L., and Tolbert, N. E. (1978) *Anal. Biochem. 87*, 206.
23. Sokoloff, L., and Rothblat, G. H. (1974) *Proc. Soc. Exp. Biol. Med. XX 146*, 1166.
24. Tanford, C., and Aune, K. C. (1970) *Biochemistry 9*, 206.
25. Sparks, D. L., Lund-Katz, S., and Phillips, M. C. (1992) *J. Biol. Chem. 267*, 25839.
26. Lehrer, S. S. (1971) *Biochemistry 10*, 3254.
27. Jameson, D. M., and Hazlett, T. L. (1991) in *Time-Resolved Fluorescence in Biology and Biochemistry. Biophysical and Biochemical Aspects of Fluorescence Spectroscopy* (Dewey, G. T., Ed.) pp 105−133, Plenum Publishing, New York.
28. Belford, C. G., Belford, R. L., and Weber, G. (1972) *Proc. Natl. Acad. Sci. U.S.A. 69*, 1392.
29. Wald, J. H., Krul, E. S., and Jonas, A. (1990) *J. Biol. Chem. 265*, 20037.
30. Davidson, W. S., Gillotte, K. L., Lund-Katz, S., Johnson, W. J., Rothblat, G. H., and Phillips, M. C. (1995) *J. Biol. Chem. 270*, 5882.
31. Sparks, D. L., and Phillips, M. C. (1992) *J. Lipid Res. 33*, 123.
32. Davidson, W. S., McGuire, K. A., and Jonas, A. in *Atherosclerosis XI. Proceedings of the XI International Symposium on Atherosclerosis* (1998) (Joctot, B., Mathe, D., and Fruchart, J. C., Eds.) pp 1135−1142, Elsevier Publishing, New York.
33. Sparks, D. L., Davidson, W. S., Lund-Katz, S., and Phillips, M. C. (1993) *J. Biol. Chem. 268*, 23250.
34. Gilardi, G., Mei, G., Rosato, N., Canters, G. W., and Finazzi-Agro, A. (1994) *Biochemistry 33*, 1425.
35. Burstein, E. A., Vedenkina, N. S., Ivkova, M. N. (1973) *Photochem. Photobiol. 18*, 263.
36. Weaver, A. J., Kemple, M. D., Brauner, J. W., Mendelsohn, R., and Prendergast, F. G. (1992) *Biochemistry 31*, 1301.
37. Meers, P. (1990) *Biochemistry 29*, 3325.
38. Thompson, R. B., and Gratton, E. (1988) *Anal. Chem. 60*, 670.
39. Jonas, A., Privat, J. P., Wahl, P., and Osborne, J. C., Jr. (1982) *Biochemistry 21*, 6205.
40. Lasagna, M., Gratton, E., Jameson, D. M., and Brunet, J. E. (1999) *Biophys. J. 76*, 443.
41. von Eckardstein, A., Funke, H., Walter, M., Altland, K., Benninghoven, A., and Assmann, G. (1990) *J. Biol. Chem. 265*, 8610.
42. Jonas, A., von Eckardstein, A., Kezdy, K. E., Steinmetz, A., and Assmann, G. (1991) *J. Lipid Res. 32*, 97.
43. Helms, M. K., Hazlett, T. L., Mizuguchi, H., Hasemann, C. A., Uyeda, K., and Jameson, D. M. (1998) *Biochemistry 37*, 14057.
44. Hazlett, T. L., Moore, K. J., Lowe, P. N., Jameson, D. M., and Eccleston, J. F. (1993) *Biochemistry 32*, 13575.
45. Rogers, D. P., Roberts, L. M., Lebowitz, J., Engler, J. A., and Brouillette, C. G. (1998) *Biochemistry 37*, 945.
46. Barbeau, D. L., Jonas, A., Teng, T., and Scanu, A. M. (1979) *Biochemistry 18*, 362.
47. Small, E. W., and Libertini, L. J. (1988) *Proc. SPIE 909, 97.*
48. Brunet, J. E., Vargas, V., Gratton, E., and Jameson, D. M. (1994) *Biophys. J. 66*, 446.
49. Marcel, Y. L., Provost, P. R., Koa, H., Raffai, E., Dac, N. V., Fruchart, J. C., and Rassart, E. (1991) *J. Biol. Chem. 266*, 3644.
50. Chen, Y. H., Yang, J. T., and Martinez, H. M. (1972) *Biochemistry 11*, 4120.

BI991428H